

# Chapter 6: Multiscale Modeling and Simulation of Deformation in Nanoscale Metallic Multilayered Composites

F. Akasheh and H.M. Zbib

School of Mechanical and Materials Engineering  
Washington State University, Pullman, WA, USA

## 6.1 Introduction

Nanoscale metallic multilayered (NMM) composites represent an important class of advanced engineering materials which have a great promise for high performance that can be tailored for different applications. Traditionally, NMM composites are made of bimetallic systems produced by vapor or electrodeposition. Careful experiments by several groups have clearly demonstrated that such materials exhibit a combination of several superior mechanical properties: ultrahigh strength reaching 1/3 to 1/2 of the theoretical strength of any of the constituent materials [28], high ductility [25], morphological stability under high temperatures and after large deformation [22], enhanced fatigue resistance of an order of magnitude higher than the values typically reported for the bulk form [35], and improved irradiation damage resistance [17, 27], again, as compared to the bulk. However, the basic understanding of the behavior of those materials is not yet at a level that allows them to be harnessed and designed for engineering applications.

The problem lies in the complexity and multiplicity of factors that govern their behavior. Although the concept of creating a stronger metal from two weaker ones by combining them in laminates has been proposed and understood by Koehler in 1970 [20], the nanometer scale introduces a new domain of complexity. At this length scale, the discrete nature of dislocations and their interactions becomes increasingly significant in dictating the response. Depending on the lattice structure and lattice parameters mismatch of the two materials, the layers can be under very high

stress states; and interfaces may contain misfit dislocation structures. The miscibility of the materials and the chemical potential strongly affect the nature of interfaces and, hence, their interaction with dislocations. The fact that interfaces form an unusually high-volume fraction of the material makes them a major factor in governing the behavior. The combined complexity and interactions among all of the above-mentioned factors explains the deficiency in the theoretical understanding of the response of NMM composites.

The strong dependence of the mechanical behavior of NMM composites on unit dislocation processes and interfaces poses a challenge to modeling and simulating their behavior. Classical plasticity does not consider the physical mechanism underlying the deformation of the modeled continuum and fails to predict the dependence of the response of metallic structures on their size. Although classical crystal plasticity provides the correct physical framework for modeling dislocation-dependent plasticity, it fails to predict size effect and related phenomena because it does not accommodate geometrically necessary dislocations associated with gradients in plastic deformation. If any, it would be strain gradient plasticity theories that could provide the suitable framework for modeling NMM composites, although this remains a challenging problem and is far from being resolved at the present state of the field.

Multiscale modeling is one of the most promising modeling paradigms which appeared in the last decade for modeling macroscopic phenomena whose roots lie at a finer scale. The approach is based on the appropriate coupling of two models for each of the scales involved. In the case of NMM composites, such coupling involves the continuum mesoscale and dislocation microscale models, although a further coupling to the atomic scale is possible but practically very complex. Three-dimensional dislocation dynamics (DD) analysis is one of the most recent and powerful tool to model the behavior of metallic materials at the microscale in a more physical manner than existing plasticity models [8, 21, 33, 40, 41]. Since its development in the early 1990s, DD analysis has made significant advancement and proved useful in addressing several problems of interest in materials science and engineering. When coupled with the continuum level finite element (FE) analysis, the result is a multiscale model of elastoviscoplasticity which explicitly incorporates the physics of dislocation motion and interactions among themselves and with external loads, surfaces, and interfaces [37, 38]. Such a model provides a very useful tool perfectly suited to studying the behavior of micro- and nanosized metallic structures. The mechanical behavior of NMM composites is clearly one example of those problems.

Section 6.2 explores the subject of modeling and simulation of NMM composites using multiscale modeling. The basics of dislocation-based metal plasticity and its mathematical modeling through DD analysis are reviewed. Multiscale coupling of continuum mechanics and dislocation dynamics are then presented. Background on the mechanical behavior of NMM composites is presented in Sect. 6.3. Finally, the benefits of multiscale and other modeling tools for NMM composites are demonstrated using different examples.

## 6.2 Multiscale Modeling of Elastoviscoplasticity

Decades of research, since the existence of dislocations in crystal was first theorized, have established that metal plasticity is governed by the response of crystal defects, mainly dislocations, to external and internal loading. Macroscopically observed deformation of metals is the cumulative result of the motion of a very large number of dislocations. Although the theory of dislocations provides a complete description of the stress, strain, and displacement fields of a dislocation as well as of their motion under the effect of forces acting on them, the extension of this theoretical understanding to provide accurate physics-based prediction of the mechanical behavior of metals is practically impossible.

A typical density of dislocation in a moderately worked metal amounts to  $10 \times 10^{12} \text{ m}^{-2}$ . A cubic millimeter of such metal contains about 1,000 m of curved dislocation lines. The huge computational demand in calculating the dynamics of such densities of dislocations, further complicated by the fact that dislocations have long-range interactions and can react with each other upon colliding to form intricate configurations with possibly new characteristics, is beyond the existing and near future computational capacities.

On the other hand, alternative continuum level modeling, although computationally feasible, remains phenomenological in nature. Even in the case of strain gradient plasticity and geometrically necessary dislocation-based theories, success of one theory in capturing certain aspects of size effects has been problem dependant; and it remains that no general framework is agreed upon. The status quo is mainly due to the complexity and multiplicity of dislocation interactions leading to size effects. For example, it is well known that a dislocation has a distortion field associated with it, which results in a long-range stress field that decays inversely proportional to the distance from the dislocation core. As the dimensions of the specimen become smaller, the interactions between

these stress fields become increasingly significant, making the nonlocal effects increasingly pronounced. Furthermore, when the dimensions of a specimen become comparable to the range of the defect structure stress field, size effect arises due to the interaction of this field with the free surfaces (image stresses).

The Hall–Petch effect, which implies that strength is inversely proportional to the square root of a characteristic microstructural length scale, e.g., the grain size in micro-sized grains or the individual layer thickness in microscale multilayered structures, can be directly attributed to dislocation pileups at grain boundaries or layer interfaces, respectively. The stress needed to activate dislocation sources also depends on the grain size and their location within the grain, which reflects as a size effect in the early stages of deformation. Another size effect originates from low-energy dislocation structures, like cell structure or dislocation walls, which tend to form by dislocation patterning and reorganization. Capturing all this complexity is a formidable task for any phenomenology-based theory.

Plasticity in metals is an example of a problem that is multiscale in nature: The macroscopically observed behavior has its origin in the complex physics occurring at the microscale. A multiscale model for plasticity would implement a continuum level framework which avoids phenomenology by explicitly incorporating the physics of plasticity at the microscale through the DD analysis. The link between the two models is two-way: the DD model calculates and passes the plastic strain and the internal stress field due to dislocations at each material point (after proper homogenization), while the continuum model accounts for boundary conditions and internal surfaces and interfaces through the solution of an auxiliary boundary value problem and the superposition concept as detailed below.

In Sect. 6.2.1, we provide a brief background on dislocations in metals. The theoretical aspects of DD and their implementation in DD simulations are presented in Sect. 6.2.2. Then the multiscale dislocation dynamics plasticity model is presented in Sect. 6.2.3.

### 6.2.1 Basics of Dislocations in Metals

Dislocations are linear defects in crystals identified by their Burgers vector and line sense. Depending on the crystal structure, a dislocation can have one out of a finite set of Burgers vectors and can glide on one of a finite set of crystallographic planes. For example, in face-centered cubic (FCC) metals, there are six possible Burgers vectors, all of  $a/2\langle 011 \rangle$ -type,  $a$  being the lattice parameter, and four  $\{111\}$  slip planes. A combination of a

Burgers vector and a slip plane defines the slip system of a dislocation. The Burgers vector defines the direction of slip of the material, while the slip plane defines the plane on which the slip motion occurs. On its plane, the dislocation can have an arbitrary line sense, which can change as the dislocation glides. Although the Burgers vector is a characteristic of a dislocation, its slip plane is not because a dislocation can change its glide plane, a process known as *cross-slip*. Dislocations glide under the effect of shear stress resolved in the slip plane along the slip direction (direction of Burgers vector). Notice the difference between slip direction, which pertains to the direction of motion of the atoms, and the dislocation line motion. The macroscopically observed plastic deformation of a metallic continuum structure is the result of the irreversible glide motion of a large number of dislocations on multiple slip systems each with its own spatial orientation. The macroscopic plastic strain tensor  $\varepsilon^p$  is thus expressed by the following relation, which reflects the tensorial addition of several multiple contributions to slip each in a certain direction  $\hat{s}^{(\beta)}$  on a particular  $\hat{n}^{(\beta)}$

$$\dot{\varepsilon}^p = \sum_{\beta} \dot{\gamma}^{(\beta)} (\hat{s}^{(\beta)} \otimes \hat{n}^{(\beta)})_{\text{sym}}, \quad (6.1)$$

where  $\dot{\varepsilon}^p$  is the plastic strain increment,  $\beta$  is the slip system index,  $\dot{\gamma}^{(\beta)}$  is the increment of slip on slip system  $\beta$ ,  $\hat{s}^{(\beta)}$  is the unit slip direction, and  $\hat{n}^{(\beta)}$  is the slip plane normal.

Gliding dislocations can also collide with each other resulting in special types of interactions (short-range interactions) which are very complicated in nature and depend strongly on the interacting dislocations' slip systems, line senses, and approach trajectory. The main interactions include annihilation, jog formation, junction formation, and dipole formation. Furthermore, dislocations can also be trapped, ceasing to move either due to short-range interactions that leave them locked or due to long-range effects like pileups against obstacles or simply due to the occurrence of regions in the material where the stress field is not high enough to drive dislocations.

## 6.2.2 DD Simulations

The idea behind conducting DD simulations is to explicitly model the behavior of a dislocation population under applied load taking into consideration all the topological and kinematical characteristics of dislocations

and their long- and short-range interactions as described above. Short-range interactions due to dislocation collision are accounted for through a set of physics-based rules learned from either atomic scale simulations or careful experimental observations. In short, DD analysis is the numerical implementation of the theory of dislocations to analyze the dynamics of a dislocation system in materials.

Generally, the simulation box in DD represents a representative volume element (RVE) of a larger specimen, although in some cases freestanding micro-sized components can make the simulation box. Unless a certain initial dislocation structure is desired, the simulation starts with a randomly generated dislocation structure. Dislocations are modeled as general curved lines in three-dimensional space made of an otherwise elastic medium characterized by its shear modulus, Poisson's ratio, and mass density. Dislocation lines are discretized into small segments, each associated with a dislocation node [39]. The nodes are the points at which forces on a dislocation from all dislocations in the system and from external loads are calculated. The governing equation for dislocation motion is then used to estimate the velocity, and hence the displacement, of each node in response to the net applied force. The node positions are updated accordingly, generating the new dislocation configuration and the process is repeated.

In this scheme, the analysis of the dynamics of continuous line objects reduces to those of a finite number of nodes. Typical to numerical algorithms, the mesh size (here the length of a segment) can be refined to obtain the desired accuracy in representing the topology of curved dislocation lines and their dynamics. The above sequence of calculations is repeated as time marches in appropriately chosen time steps, to the desired point of evolution of the dislocation system or the overall stress or strain levels. The details of the approach outlined above will be explored in the following section.

### ***Dislocation equation of motion***

The theory of dislocations provides the following governing equation for the motion of a straight dislocation segment  $s$  [11, 14, 18]:

$$m_s \dot{v}_s + \frac{1}{M_s} v = F_s. \quad (6.2)$$

Typical of a Newtonian-type equation of motion, it expresses the relation between the velocity of "an object" and the dislocation segment of effective mass  $m_s$ , moving in a viscous medium with a drag coefficient of

$1/M_s$  under the effect of a net force  $F_s$ . The effective mass per unit dislocation length  $\tilde{m}$  has been given for the edge and screw components of a dislocation as follows [14]:

$$\tilde{m}_{\text{edge}} = \frac{W_0 C^2}{\nu^4} (-16\gamma_1 - 40\gamma_1^{-1} + 8\gamma_1^{-3} + 14\gamma + 50\gamma^{-1} - 22\gamma^{-3} + 6\gamma^{-5}) \quad (6.3a)$$

and

$$\tilde{m}_{\text{screw}} = \frac{W_0}{\nu^2} (-\gamma^{-1} + \gamma^{-3}) \quad (6.3b)$$

with  $\gamma = \sqrt{1 - (\nu/C)^2}$  and  $\gamma_1 = \sqrt{1 - (\nu/C_1)^2}$ .  $C$  and  $C_1$  are the transverse and longitudinal sound speeds in the elastic medium,  $\nu$  is the dislocation speed, and  $W_0$  is the line energy of a dislocation per unit length given as  $W_0 = (Gb^2/4\pi) \ln(R/r_0)$  [13]. In the later expression,  $G$  is the shear modulus,  $b$  is the magnitude of the Burgers vector, and  $R$  and  $r_0$  are the external and internal cutoff radii, respectively.  $M_s$  is the dislocation mobility and it is typically a function of temperature and pressure. The net force  $F_s$  acting on a dislocation line can have several contributions to it depending on the problem. In general,

$$\begin{aligned} F_s = & F_{\text{Peierls}} + F_{\text{dislocation}} + F_{\text{self}} + F_{\text{external}} + F_{\text{obstacle}} \\ & + F_{\text{image}} + F_{\text{osmotic}} + F_{\text{thermal}}, \end{aligned} \quad (6.4)$$

where  $F_{\text{Peierls}}$  is the force from lattice friction opposing the motion of a dislocation,  $F_{\text{self}}$  is the force from the two neighboring dislocation segments directly connected to the segment under consideration,  $F_{\text{dislocation}}$  is the net force from all other dislocation segments in the simulation domain,  $F_{\text{external}}$  is the force due to externally applied loads,  $F_{\text{obstacle}}$  is the interaction force between a dislocation and the stress field of an obstacle,  $F_{\text{image}}$  is the force experienced by a dislocation due to its presence near free surfaces or interfaces separating phases of different elastic properties,  $F_{\text{osmotic}}$  is the driving force in climb, and  $F_{\text{thermal}}$  is the force on the dislocation from thermal noise. In general, the force due to a general stress field  $\sigma$  is given by

$$F_s = l_s \sigma \cdot b_s \times \xi_s, \quad (6.5)$$

where  $l_s$  is the segment length and  $\sigma$  is the stress field ‘‘felt’’ by the dislocation segment, while  $b_s$  and  $\xi_s$  are the Burgers vector and the line sense, respectively, of the dislocation segment. For example, in the case of

externally applied loads, the relevant stress field is  $\sigma^a$ , the net stress from all external loads along segment  $s$  and its force contribution will be  $F_{\text{external}} = l_s \sigma^a \cdot b_s \times \xi$ . The details of the calculation of  $F_{\text{dislocation}}$  and  $F_{\text{self}}$  are not trivial and will be further detailed below.

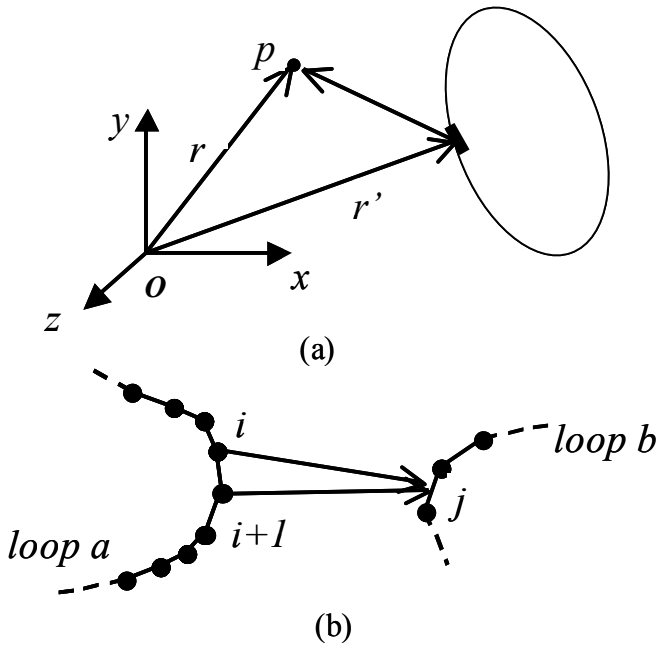


**Fig. 6.1.** (a) Integration of the stress field at a point  $p$  due to a dislocation loop and (b) the corresponding integration in the framework of DD by the linear element approximation

**Evaluation of  $F_{\text{dislocation}}$**

As mentioned above, this force contribution comes from all of the dislocation segments in the system except for those two connected to the dislocation node under consideration. Dislocation theory provides the stress field of an arbitrary dislocation loop  $C$  at an arbitrary point  $p$  defined by the position vector  $r$  through the following expression [13] (see Fig. 6.1a).

$$\begin{aligned} \sigma_{\alpha\beta} = & -\frac{G}{8\pi} \oint_C (b \times \nabla') \frac{1}{R} \otimes dl' + \frac{G}{4\pi} \oint_C dl' \otimes (b \times \nabla') \frac{1}{R} \\ & - \frac{G}{4\pi(1-\nu)} \oint_C \nabla' \cdot (b \times dl') (\nabla \otimes \nabla - I \nabla^2) R, \end{aligned} \quad (6.6)$$

where  $\mathbf{R}$  is position vector of  $p$  relative to the dislocation segment position  $\mathbf{r}'$  and  $I = \mathbf{e}_1 \otimes \mathbf{e}_1 + \mathbf{e}_2 \otimes \mathbf{e}_2 + \mathbf{e}_3 \otimes \mathbf{e}_3$  is the unit dyadic. In the numerical implementation, dislocation curves are discretized into linear segments; and the above integrals over closed loops become sums over linear segments of length  $l_s$ ; and the contribution from all segments is summed up to find the stress field at any desired point  $p$

$$\sigma_{\alpha\beta} = \sum_{s=1}^{N_s-2} \left\{ \begin{array}{l} -\frac{G}{8\pi} \int_s (b \times \nabla') \frac{1}{R} \otimes dl' + \frac{G}{4\pi} \int_s dl' \otimes (b \times \nabla') \frac{1}{R} \\ -\frac{G}{4\pi(1-\nu)} \int_s \nabla' \cdot (b \times dl') (\nabla \otimes \nabla - I \nabla^2) R \end{array} \right\}. \quad (6.7)$$

Furthermore, the integration over the segment length can be evaluated algebraically using the linear element approximation found in [3, 13]. According to this approach, the stress field at point  $p$  from a dislocation segment bound by nodes  $i$  and  $i+1$  can be evaluated as [39] (see Fig. 6.1b)

$$\sigma_{\alpha\beta}(p) = \sigma_{\alpha\beta}^{i+1} - \sigma_{\alpha\beta}^i. \quad (6.8)$$

### Evaluation of $F_{self}$

When applied to calculate the stress field at dislocation node  $j$  which belongs to the same dislocation segment whose stress contribution is being considered, the above procedure does not work due to the singular nature of the stress field at the dislocation core. To overcome this obstacle, a regularization scheme developed in [41] is implemented. Consider the dislocation bend consisting of a semi-infinite line and segment  $(j, j+1)$ , as shown in Fig. 6.2a. The glide force per unit length acting on a point on segment  $(j, j+1)$  at a distance  $\lambda$  is explicitly given for the case where the adjacent segment is semi-infinite in length as [13]

$$\frac{F_g}{L} = \frac{G}{4\pi\lambda} f_g(\theta, b). \quad (6.9)$$

This expression can be used to find the average force per unit length on segment  $(j, j + 1)$  by integrating it over the length of the segment yielding

$$\left(\frac{F_g}{L}\right)_{\text{avg}} = \frac{G}{4\pi L} f_g(\theta, b) \left( \ln\left(\frac{L}{b}\right) + \beta \right), \tag{6.10}$$

where  $\beta$  is an adjustable parameter that compensates for the energy contained in the dislocation core. Equation (6.10) is an equivalent expression to an alternative expression where an adjustable core cutoff radius  $r_0$  is used. To adapt the above solution to the case of a finite segment  $(j - 1, j)$ , the superposition principle is used and the net glide component of the force on segment  $(j, j + 1)$  due to segment  $(j - 1, j)$  can be found by subtracting, from (6.10), the interaction force between additional semi-infinite segment and  $(j, j + 1)$  calculated using the standard procedure (Fig. 6.2b).

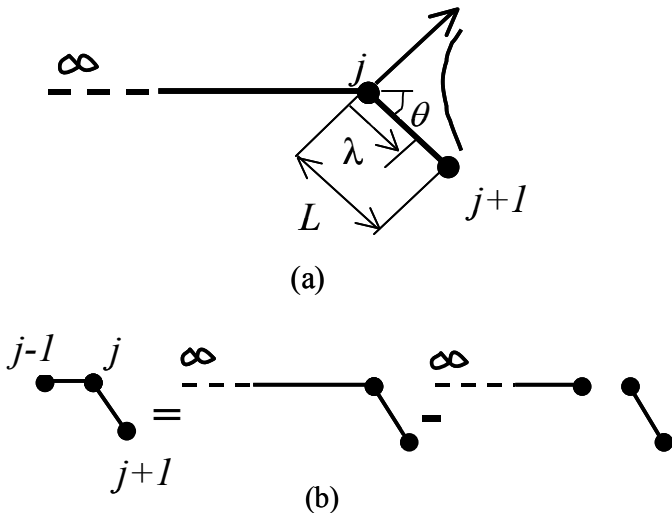


**Fig. 6.2.** Calculation of the Peach–Koehler force on a dislocation segment due to its direct neighboring segment

**Treatment of boundary conditions**

Typically, the simulation box used in DD analyses is an RVE representative of an infinite medium. To account for this model, special boundary conditions are needed. Two types of boundary conditions are applied in DD (1) reflection boundary conditions, which ensure the continuity of dislocation curves [41] and (2) periodic boundary conditions, which ensure both the

conservation of the dislocation flux and the continuity of the dislocation curves [2].

As for the cases where the simulation box represents the complete specimen with finite domain and arbitrary loading conditions, the above boundary conditions are no longer valid; and a special treatment for the finite domain is needed. This treatment is implemented within the framework of the multiscale model and its discussion is presented in Sect. 6.2.3.

### ***Evaluation of the macroscopic plastic strain***

In metals, macroscopic deformation is the result of slip on different slip systems. The area swept by a gliding dislocation represents the area of the newly slipped region due to this motion. In the framework of DD, the increment of the plastic strain can be explicitly calculated from the area swept by the dislocation segments using this relation [39]

$$\dot{\epsilon}^p = \sum_{s=1}^{N_s} \frac{l_s v_s}{2V} (n_s \otimes b_s + b_s \otimes n_s), \quad (6.11)$$

where  $N_s$  is the total number of dislocation segments,  $l_s$  is the segment length,  $v_s$  is the segment glide velocity,  $b_s$  is the segment Burgers vector,  $n_s$  is the normal to the slip plane of the segment, and  $V$  is the volume of the RVE.

### **6.2.3 Multiscale DD Model**

The coupling of continuum mechanics and DD calculations provides the physical link between the meso- and the microscales. At the continuum level, the typical laws governing an elastic continuum are implemented along with Hooke's law for the elastic regime, as usual. No constitutive law for the plastic behavior of the material is prescribed. Instead, the continuum level plastic strain is explicitly calculated from the actual motion of the underlying dislocations and homogenized at each material point.

Another quantity that is explicitly calculated in DD and passed to the continuum scale is the internal stress from dislocations (and any other defects exhibiting long-range, self-induced stress fields). In this manner, the continuum level back-stress concept and its direct effect on hardening are naturally incorporated. Furthermore, this framework allows the rigorous treatment of boundary conditions for free surfaces and interfaces separating

heterogeneous media through the concept of image stresses and eigenstresses, respectively, as will be demonstrated below. This framework also facilitates the application of general loading conditions in DD simulations.

**Treatment of finite domains**

The stress fields employed in the DD calculations are those for a dislocation in infinite homogeneous media. In the case of finite domains, the stress fields are truncated at the boundaries and, thus, the dislocation can experience a force depending on its position relative to the free surfaces. The stress field calculations in this situation can be handled through the concept of superposition [5, 34, 39]. The elastic fields for the finite domain problem can be found by summing the elastic fields from two solutions: that for the dislocations as if they existed in an infinite medium, and the solution to a complementary problem where the domain is finite and tractions equal but opposite to those caused by the infinite stress fields at the finite domain boundary (Fig. 6.3)

$$\begin{aligned}
 u^D &= u^{D\infty} + u^* , \\
 \varepsilon^D &= \varepsilon^{D\infty} + \varepsilon^* , \\
 \sigma^D &= \sigma^{D\infty} + \sigma^* ,
 \end{aligned}
 \tag{6.12}$$

where the superscript  $D\infty$  indicates a defect field quantity as if the defect existed in an infinite homogeneous medium, while the superscript  $*$

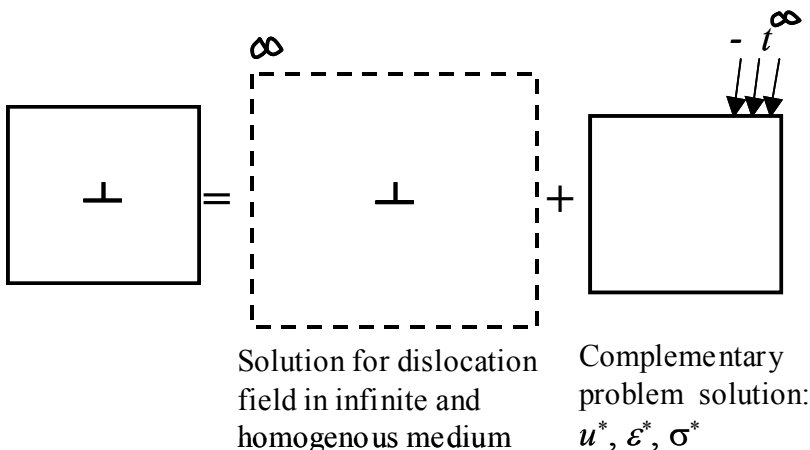


**Fig. 6.3.** Superposition principle application for the rigorous treatment of finite boundaries

indicates the solution to the complementary problem described above and satisfying the following boundary conditions:

$$\begin{aligned} t &= t^a - t^{\infty 1} - t^{\infty 2}, & \text{on } \partial\Omega, \\ u &= u^a, & \text{on } \partial\Omega_u. \end{aligned} \tag{6.13}$$

Here,  $t^a$  and  $u^a$  represent any externally applied tractions and any prescribed boundary displacements, respectively, on their corresponding parts of the boundary.

**Treatment of heterogeneous media**

Consider the infinite domain  $\Omega$  consisting of two subdomains  $\Omega_1$  and  $\Omega_2$ . Both  $\Omega_1$  and  $\Omega_2$  contain dislocations and other defects. The stress field in each medium  $\sigma_{\Omega_1}$  and  $\sigma_{\Omega_2}$  can be expressed as follows [39]

$$\begin{aligned} \sigma_{\Omega_1} &= \sigma^{D\infty 1} + \sigma^{D\infty 2} + \sigma^{\infty 12}, \\ \sigma_{\Omega_2} &= \sigma^{D\infty 2} + \sigma^{D\infty 1} + \sigma^{\infty 21}, \end{aligned} \tag{6.14}$$

where  $\sigma^{D\infty 1}$  and  $\sigma^{D\infty 2}$  are the stress fields due to the defect structure as if the whole domain were homogenous and made of the material of  $\Omega_1$  and  $\Omega_2$ , respectively.  $\sigma^{\infty 12} = [C_1 - C_2]\varepsilon^{D\infty 2}$  and  $\sigma^{\infty 21} = [C_2 - C_1]\varepsilon^{D\infty 1}$  represent the image stress due to the difference in the elastic properties.

**Treatment of the general case**

Consider a finite domain  $\Omega$  consisting of two subdomains  $\Omega_1$  and  $\Omega_2$ . Each medium can have its own dislocation (and possibly other defects) structure which exhibits long-range effects. The total elastic fields can be expressed as the sum of four solutions (1) that for dislocations in  $\Omega_1$  as if they existed in an infinite medium made of the  $\Omega_1$  material, (2) that for the dislocations in  $\Omega_2$  as if they existed in an infinite medium made of the  $\Omega_2$  material, (3) the image fields due to the difference in elastic properties of the two media, and (4) the solution to a complementary problem where the domain is finite and traction equal but opposite to that caused by the infinite stress fields at the finite domain boundary, as described before. Furthermore, any externally applied loads can be included in the complementary problem [39]

$$\begin{aligned} \sigma_{\Omega_1} &= \sigma^{D\infty 1} + \sigma^{D\infty 2} + \sigma^{\infty 12} + \sigma^{*1}, \\ \sigma_{\Omega_2} &= \sigma^{D\infty 2} + \sigma^{D\infty 1} + \sigma^{\infty 21} + \sigma^{*2}, \end{aligned} \tag{6.15}$$

where  $\sigma^{*1} = [C_1]\varepsilon^*$  and  $\sigma^{*2} = [C_2]\varepsilon^*$ , and  $\varepsilon^*$  is the solution for the complementary problem where the finite domain is subjected to the following boundary conditions

$$\begin{aligned} t &= t^a - t^{\infty 1} - t^{\infty 2}, & \text{applied to } \partial\Omega, \\ u &= u^a, & \text{applied to } \partial\Omega_u, \end{aligned}$$

where  $t$  and  $u$  denote traction and displacement, the superscript  $a$  denotes externally applied quantities, and  $\partial\Omega_u$  is the part of the boundary to which external displacement boundary conditions are applied.

**Finite element implementation**

From the continuum point of view, the simulated material consists of an elastic medium with internal defect structure. The macroscopic behavior is governed by the basic laws of continuum mechanics. If a small strain deformation is assumed, then the total strain  $\varepsilon$  can be decomposed into an elastic part  $\varepsilon^e$  and a plastic part  $\varepsilon^p$  as follows:

$$\begin{aligned} \varepsilon &= \frac{1}{2}(\nabla u + u\nabla), \\ \varepsilon &= \varepsilon^e + \varepsilon^p. \end{aligned} \tag{6.16}$$

Furthermore, if Hooke’s law is used as the constitutive law for the elastic regime, then one can write  $\sigma = C[\varepsilon - \varepsilon^p]$ . Depending on the problem, the stress  $\sigma$  can have any of the contribution to stress mentioned above. In the most general case,

$$\sigma_{\Omega_i} = \sum_{i=1}^N \sigma^{D\infty i} + \sum_{j=1}^N [C_i - C_j]\varepsilon^{\infty ij} + [C_i]\varepsilon^* \tag{6.17}$$

with  $N$  being the number of subdomains making the structure and  $\varepsilon^*$  the solution for the complementary problem with boundary conditions:

$$\begin{aligned} t &= t^a - \sum_{i=1}^N t^{\infty i}, & \text{on } \partial\Omega, \\ u &= u^a, & \text{on } \partial\Omega_u. \end{aligned} \tag{6.18}$$

The finite element formulation for the above problem results in the following [37, 39]

$$[M]\{\ddot{u}\} + [C]\{\dot{u}\} + [K]\{u\} = \{F^a\} + \{F^\infty\} + \{F^B\} + \{F^P\}, \quad (6.19)$$

where  $[M]$ ,  $[C]$ , and  $[K]$  are the global mass, damping, and stiffness matrices, respectively.  $\{F^a\}$  and  $\{F^\infty\}$  represent, respectively, the externally applied force vector and the force vector from tractions on the free surfaces due to the truncations of the long-range dislocation fields. The body force vector  $\{F^B\}$  results from the long-range stress fields in the dislocations (and other defects if present), i.e., the contribution of the  $\sigma^{D\infty}$  terms. If present,  $\{F^B\}$  also includes the contribution of the image forces due to the difference in the elastic moduli of the different subdomains, i.e., the second term on the right-hand side of (6.17). It is through  $\{F^B\}$  that the long-range effect of dislocations belonging to any of the finite elements in the mesh on the dislocation in a certain element is considered. As for the interactions between the dislocations belonging to the same element, the interactions are calculated explicitly as described in Sect. 6.2.2. Finally,  $\{F^P\}$  reflects the contribution of the stress term resulting from  $\varepsilon^P$ .

### 6.3 Nanoscale Metallic Multilayered Composites

NMM composites are typically produced by physical vapor deposition. The microstructure and mechanical properties of the composite are not only dependent on the absolute properties of the individual constituent metals, but also on their relative values (for example their lattice parameters and elastic properties mismatch) and on the individual layer thickness. Furthermore, the deposition process parameters sensitively affect the properties of the resulting structure.

A fundamental classification of the type of NMM systems, hence their behavior, is based on the compatibility of slip systems in the two phases and is commonly used. Coherent systems exhibit “almost” continuous slip systems across the interfaces such that dislocations gliding on a certain slip plane in one layer can continue to glide on the same plane in the neighboring layer. This condition requires the two metals to exhibit the same lattice structure, a small lattice parameter mismatch, and to be deposited epitaxially. Other terminology used to describe such systems is

“transparent interface” systems [16]; transparent in the sense that dislocations can cross the interface into the neighboring material.

On the other hand, in incoherent systems, also known as “opaque interface” systems, slip systems in the two phases do not match, which means that dislocations cannot continue to glide in the neighboring layers. Instead, interfaces can act as slip barriers through different mechanisms. For example, in the Cu/Nb FCC/BCC system, interfaces act as sinks for interlayer dislocations as they enter the interface and their core spreads [15]. Incoherent systems involve metals with different crystal structure or ones with similar crystal structure but with large lattice parameters mismatch or large lattice misorientation.

Interface crossing is a critical plasticity propagation process in NMM composites because it marks the end of confined layer slip and the spread of dislocation activity in both phases of a coherent system, defining the limit of strength. In this work, the discussion will be limited to the strength of NMM composites made of coherent systems, in particular the FCC–FCC Cu/Ni system with {100} interface. This orientation is also known as cube-on-cube. The lattice parameters of Cu and Ni are 0.3615 and 0.3524 Å amounting to a small mismatch of 2.6%, which allows for continuous slip between the Cu and Ni layers. Furthermore, we will restrict the discussion to the effect of the layer thickness on the mechanical and structural properties of NMM composites.

An investigation of the strength of NMM composites should start by studying the stress relaxation process of the as-deposited composite. The relaxation process dictates the nature of the initial dislocation structure, the interface properties, and the internal stress state in the composite. In turn, this as-deposited structure influences the ultimate mechanical response under loading. Due to its critical role, a brief discussion of stress relaxation in coherent multilayered systems should be in place at this point. The epitaxial coherent growth of two different materials forces the atomic positions of the materials to coincidence in spite of the slight difference in lattice parameters and atomic positions. For coherency to be maintained, the lattice with the larger size has to compress while that with the smaller size has to expand for them to match. The result is a strained multilayer structure having coherency strains and stresses of alternating sign (tension/compression). Coherency stresses can be extremely high, measuring about 2.6 GPa in the case of Cu/Ni system [16]. Consequently, as the deposition process proceeds, the structure’s elastic energy increases linearly with the increase in thickness. At a certain point, it becomes energetically favorable for the system to reduce its elastic energy by injecting dislocations resulting in a semicoherent structure whose overall energy is less.

A critical layer thickness  $h_c$  is identified below which the structure is coherent and made of strained layers and above which the structure is semicoherent and has a network of interfacial dislocations and a reduced level of coherency stresses [6, 23, 24]. The relaxation process proceeds by the glide of what is known as threading dislocations. Threading dislocations are glide dislocations that originate from faults in atomic arrangement occurring during the deposition process. Once generated in one layer, they continue to replicate themselves in the layers deposited thereafter maintaining the same slip system. When the layer thickness is above the critical thickness, the resolved shear stress component of the coherency stresses drives the threading dislocations along their slip planes while the alternating stress state acts to confine them to their respective layers. This glide process is known as the *Orowan bowing* and results in the common hairpin dislocation structure (Fig. 6.4).

Another suggested source of dislocations is the nucleation of half-loops from free surfaces followed by their propagation within the layer [19]. Furthermore, in the process of threading, dislocations can interact with other threading dislocations or interfacial dislocations deposited by earlier threading events. Cross-slip is commonly observed in NMM composites and provides another dislocation multiplication mechanism. Threading dislocations can also react with each other to form Lomer locks which are commonly observed in an increasing number as the layer thickness increases [25, 29, 30].

The end result of all these interactions among dislocations and between dislocations and the evolving stress field is a structure with a complex network of interfacial dislocations (including glide dislocations, sessile Lomer-type dislocations, and dislocation bends), blocked threading dislocation, dislocation junctions, and jogs along with a remanent nonuniform distribution of internal stresses. The presence of “residual” internal stress in the structure is a consequence of the fact that full relaxation removing all coherency stresses is practically impossible due to several factors that impede the relaxation process. Such factors include dislocation–dislocation interactions, lattice friction, and the existence of other defects, all of which act to block the motion of threading dislocations. Even if the misfit dislocation network necessary to minimize the system energy is imagined to exist, there will still be a nonzero internal stress due to the stress fields of these dislocations.

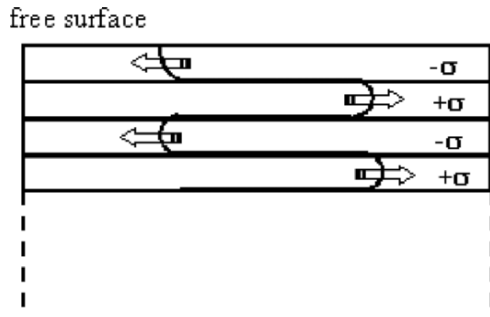


**Fig. 6.4.** The glide of a threading dislocation in different layers

The equilibrium semirelaxed structure described above becomes the initial structure for the consequent loading of the composite in service. If the applied load is high enough, it will provide the necessary driving force for dislocation activity to resume, with the softer layer flowing first. Meanwhile, the harder layer would be under elastic loading; and the laminate structure, as a whole, is still capable of supporting increased loading levels due to the hard phase still being in the elastic regime. For the overall structure to yield, both layers have to deform plastically. One scenario leading to this is the crossing of the dislocations from the soft layer to the harder one.

As outlined in the previous discussion, the basic model to describe the primary plasticity mechanism in NMM composites is that of Orowan bowing of a threading dislocation. Based on this, model expressions for the critical thickness and strength of layered composites were developed by [6, 23] and further elaborated and modified by several researchers. From a mechanistic point of view, the idea is based on the balance between the force exerted by the misfit stress on the threading dislocation and the tension force in the created dislocation lines. By equating those forces, one finds the channeling stress dependence on layer thickness to be proportional to  $\ln(h)/h$ ,  $h$  being the layer thickness. The same results can be arrived at through an energetic approach.

This simple model, however, underestimates the measured strength of NMM composites as well as  $h_c$ . This is not surprising because the Orowan bowing model does not account for the effect that the presence of other dislocations in the system has on the critical condition for the stability of a threader. This effect can be due to long-range interactions as well as short-range interactions. Other proposed reasons for this discrepancy include

barriers to dislocation nucleation, kinetic effects, Peirels friction, step formation at surfaces and interfaces, and Koehler forces resulting from elastic properties mismatch. This work will focus on the effect of the dislocation–dislocation interaction (both long and short range) on the strength of NMM composites.

Considering a network of interfacial dislocations rather than a single dislocation, several authors developed energy expressions for stable dislocation arrays in multilayered systems as a function of layer thickness [4, 9, 10, 12, 36]. Although these models are more realistic and resulted in improved  $h_c$  and strength predictions, they are based on simple configurations where the dislocations in the array are equally spaced and infinite in length. In real situations, however, those assumptions are rarely representative of the dislocation networks distribution.

To understand the strengthening effect of predeposited interfacial dislocations on the stress needed to drive a threading dislocation, hereafter referred to as the *channeling stress* [31], Freund [7] considered the effect of glide interfacial dislocations that intersect the path of a threading dislocation in an unpassivated film. It was concluded that the presence of an interfacial dislocation forces the threading dislocation to “squeeze” through a narrowed-down channel with effective thickness  $h^*$  as opposed to the actual layer thickness  $h$ . A blocking criterion was suggested based on this analysis, which predicts a significant hardening effect due to this interaction. For thicknesses below 100 nm, this effect was about 50%. Using Freund’s approach, Nix [31] evaluated the effect of passivation and elastic properties mismatch between the film and the substrate on the channeling strength. For the case of unpassivated film with “very rigid” substrate, the channeling strength increased by 30% over the reference (no interfacial dislocations present) strength for the same film thickness. For the case of  $10b$  ( $b$ : magnitude of Burgers vector) thick passivation layer and uniform elastic properties for the film, passivation, and substrate, the strength increase was about 50%.

In Freund’s calculations, the interfacial dislocation was assumed to be a straight and pinned line not allowed to undergo short-range interactions. Furthermore, the threading dislocation was considered to be made of one straight segment, while the critical passing point, corresponding to the effective channel thickness  $h^*$ , was assumed to occur directly above the interfacial dislocation. As will be seen, these assumptions make this model far displaced from a real-life scenario. In fact, the blockage mechanism is completely absent in NMM composites when the interfacial dislocation is of the glide type and short-range interactions become the main factor that dictate the outcome of this process.

In an attempt to make more realistic predictions of the strength of nanoscale multilayered systems, Misra et al. [26] developed a model based on the Orowan bowing for a single threading dislocation in a layer having equally spaced interfacial dislocations and extended it to include the resistance to dislocation crossing from one layer to the next through the interface. Using an energy approach, the stress needed to propagate the hairpin was estimated for two bounding cases. In the upper bound case, the threading dislocation was assumed to propagate in the presence of an array of equally spaced interfacial Lomer-type dislocations as well as “left over” unrelaxed coherency stress inversely proportional to the layer thickness. In the lower bound case, the dislocation array was ignored. In both cases, the interfacial dislocation arrays were assumed to be the source of resistance to dislocation crossing into the neighboring layer. For yield to occur, the applied stress must be sufficiently large to propagate the threading dislocation and overcome the interface resistance. Lower bound estimates with the proper choice of the core size produced a good match to the experimental data for the strength of Cu–Ni systems.

The above discussion demonstrates the strong dependence of the mechanical response of NMM composites on the underlying dislocation structure and its interactions with interfaces and free surfaces. The discussion also pointed out that, in spite of their better predictions and insightfulness, analytical models developed to predict the behavior of NMM composites remain far from capturing the complexity of real systems. DD provides the right framework to address such problems because it treats dislocations and their interaction explicitly. Furthermore, the multi-scale coupling of DD with continuum mechanics allows the rigorous treatment of surfaces and interfaces at the macroscale.

Nevertheless, care should be exercised when interfaces are modeled in the DD framework. The physics of interfaces and their interactions with dislocation are very complicated and should be addressed at the atomic level. Another limitation to DD analysis in the modeling of NMM composites is the lower bound on layer thicknesses which can be accurately handled. As the layer thickness decreases, the length of the segments must also decrease for the accurate representation of dislocation curves. However, the segment length can become so small so as to permit the overlap of dislocation cores where the linear elasticity solution is not defined.

## 6.4 Modeling and Simulation of NMM Composites: Examples

The ultimate goal of modeling NMM composites is to provide accurate predictions for their mechanical response under various loading conditions. The achievement of this goal is important for the design of NMM composites for different engineering applications. Due to the complexity of the physics of NMM composites, this goal has been elusive to analytical approaches. The use of DD to study plasticity mechanisms in NMM composites and how they contribute to the macroscopically observed response will be demonstrated in this section.

We start by considering the modeling of four significant unit processes in isolation from other effects which inevitably exist in real systems (1) the basic Orowan bowing process, (2) the interaction between a threading dislocation and orthogonal interfacial dislocations intersecting its glide path, (3) the interaction between a threading dislocation and parallel interfacial dislocations, and (4) threading in a surface layer. Next, the collective behavior of a system of dislocations as in real-life scenarios will be discussed. In these simulations, all the above-mentioned unit processes, and others, naturally interplay and lead to the overall response of the composite.

### 6.4.1 Modeling of Unit Dislocation Process in NMM Composites

In complex systems where many mechanisms interact to produce the overall behavior, it seems plausible to disseminate the complexity by identifying a number of mechanisms thought to be significant and investigating them one at the time and in isolation of any other mechanisms. The next question becomes that of appropriately combining their behavior in a statistical manner to arrive at the overall behavior. This involves not only the statistics of each process individually, but also possible correlations among them. The benefits of investigating, within the framework of multiscale DD, a number of such significant and frequently occurring dislocation processes in NMM composites are demonstrated.

#### ***Orowan bowing***

Figure 6.5 shows the crystallography of the problem and the setup used to model the Orowan bowing in a confined layer. It consists of a  $\{001\}$  orientation Cu layer with rigid walls. The physical properties of Cu used in this calculation and all the ones to follow in this work are listed in

Table 6.1. This layer represents a single buried layer in an infinite elastic medium of the same properties as that of the material of the layer, which implies that no image forces exist. Slip is confined to the layer by its rigid walls impenetrable by dislocations. An infinite  $a/2\langle 011 \rangle$   $\{111\}$ -type dislocation resides on its slip plane with that portion contained in the layer representing the threading dislocation. If the stress applied to the layer is sufficiently high, the dislocation will bow out. Channeling stress defines the minimum stress needed to cause the dislocation to bow out indefinitely (i.e., become unstable).

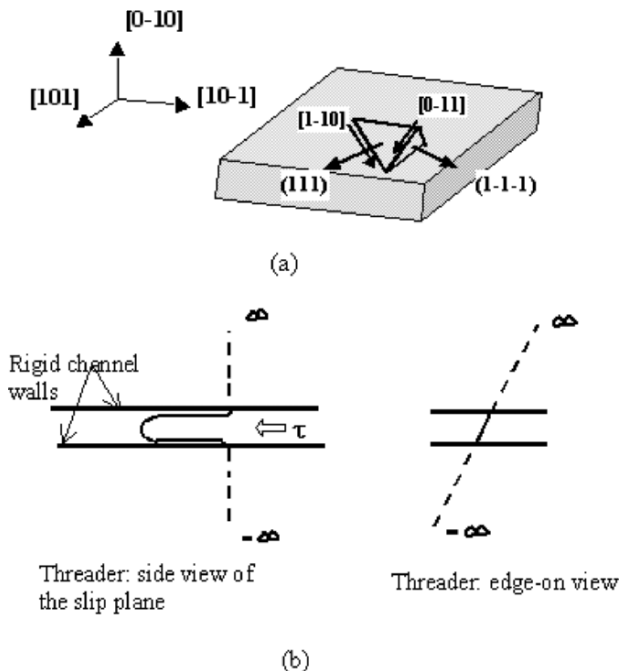
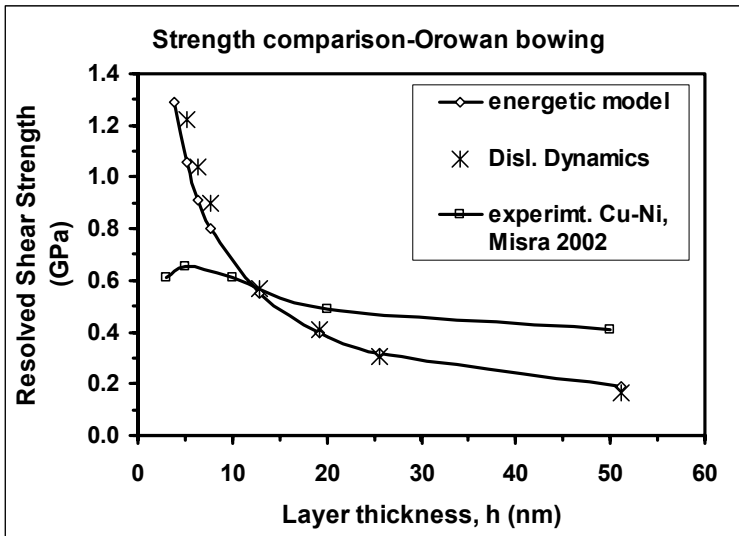


**Fig. 6.5.** (a) Crystallographic orientation of the layer and (b) setup for Orowan bowing simulation: infinite  $a/2\langle 011 \rangle$ -type dislocation with a portion contained in a rigid channel subject to stress such that the dislocation threads in its slip plane

**Table 6.1.** Physical properties of Cu used in DD calculations

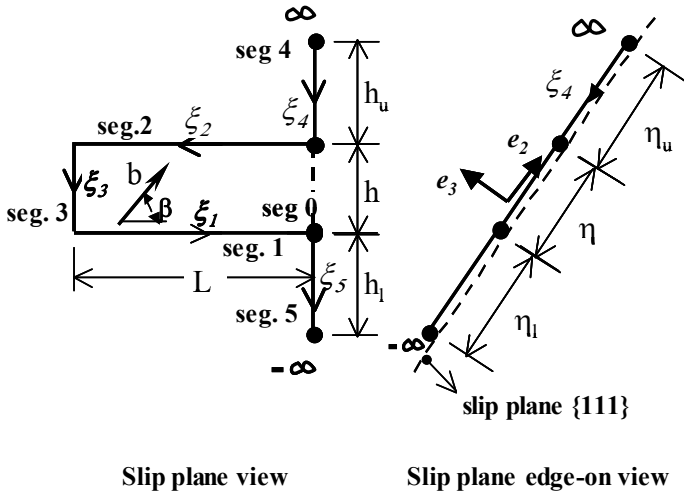
Density ( $\text{Kg m}^{-3}$ )	8,980.0
Burgers vector magnitude ( $\text{\AA}$ )	2.556
Shear modulus (GPa)	38.46
Poisson's ratio	0.3
Core size ( $b$ : Burgers' vector magnitude)	1.0
Mobility ( $1 \text{ Pa}^{-1} \text{ s}^{-1}$ )	$1.0 \times 10^4$

Figure 6.6 shows the DD prediction of the channeling stress as a function of layer thickness. The numerical parameter  $\beta$  in (6.10) was determined to be 0.5 through a fitting procedure for the DD results so that they match the corresponding stress obtained from an analytical model based on dislocation interaction energies in the system (see Fig. 6.7). As expected, the channeling strength increases as the layer thickness decreases.



**Fig. 6.6.** Comparison of the strength due to Orowan bowing as predicted by DD and the energetic model (Fig. 6.7) with the measured strength of Cu/Ni multilayered structure

Also plotted in Fig. 6.6 is the measured strength of a real Cu/Ni system. Although the model bears little resemblance to the real system, the mild difference between the elastic moduli of Cu and Ni makes the comparison reasonable due to the minor effect of image force in such a system. This, however, does not apply for the few nanometer thickness range as the interface-related mechanism dominates over Orowan bowing [26]. This is why both DD and the analytical model results continue to predict increasing channeling strength in this range while the real system shows saturation followed by softening. Outside this range, both models underestimate the strength of a multilayer system. This should not be a surprise since a model based on a single bowing dislocation is not expected to capture the interactions between bowing dislocations and other bowing



**Fig. 6.7.** Dislocation configuration modeling the threading process in a confined layer

dislocations and/or predeposited interfacial dislocations. This leads us to consider the DD simulation of the next two mechanisms.

### ***Interaction between threading and orthogonal interfacial dislocations***

The encounter between a threading dislocation and an interfacial dislocation orthogonally intersecting its path should be a very common event given the biaxial nature of loading in NMM composites. Freund [7] studied this interaction mechanism and developed the blockage model along with the associated concept of the effective channel thickness. As mentioned in the introductory part of this section, DD analysis indicates that the assumptions underlying this model suppress the possibility of short-range dislocation interactions making this model unrealistic. In fact, DD simulations [1] indicate that short-range interactions dictate the outcome of this type of interaction and that the blocking mechanism is not realistic all together in the case of a threader's encounter with glide-type interfacial dislocations.

In the case of an encounter between a threading dislocation and nonreacting Lomer-type dislocations, the blockage mechanism is realistic and has been observed. Nevertheless, the assumptions underlying the blockage mechanism are still coarse. In the process of bypassing an intersecting Lomer-type interfacial dislocation, the threader tends to adjust its configuration in a complex dynamic manner so as to minimize the overall system energy, rendering unclear the notion of  $h^*$  and a narrowed-down

channel right above the obstacle through which the dislocation “squeezes-in” to overcome the stress field. Figure 6.8 shows simulation snapshots for the dynamic process of leading a threader to bypass a Lomer-type obstacle.

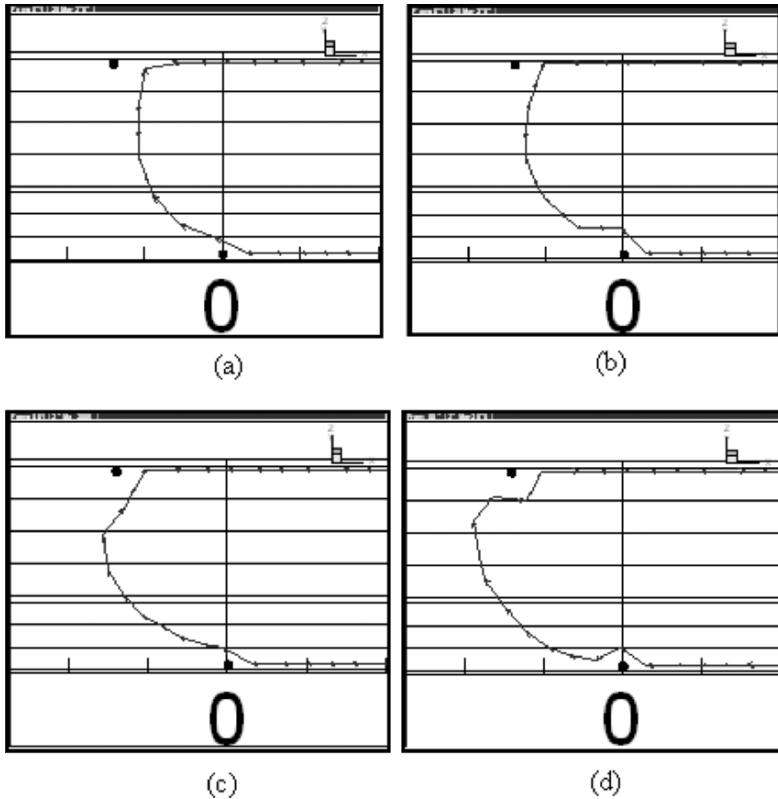


**Fig. 6.8.** Snapshots ((a)–(d) ordered in increasing simulation time) from DD simulations showing the complex sequence of configurations by which a threading dislocation bypasses a Lomer-type dislocation at the interface

As mentioned above, short-range dislocation interactions dominate the outcome of the encounter between threading and predeposited interfacial dislocations. Depending on the particular slip systems of the threader and the interfacial dislocation involved in the four representative encounters dictated by the crystallographic nature of the problem (Fig. 6.9), annihilation or jog formation can occur. Simulations indicate that the strongest effect on the strength is that of the annihilation interaction occurring when the Burgers vectors of both dislocations are collinear [1].

Figure 6.10 shows the channeling stress dependence on layer thickness as modified by this process. In the plot, the measured strength of Cu/Ni NMM composite and the reference strength due to the basic Orowan

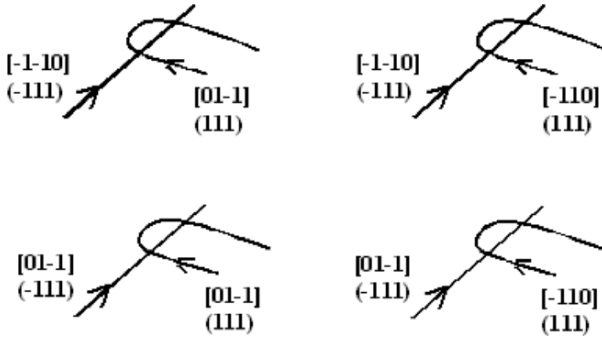


Fig. 6.9. The four encounters representing all possible intersections between threading dislocation and  $a/2\langle 011 \rangle$ -type interfacial dislocation dipoles (same crystallographic setup as that shown in Fig. 6.5)

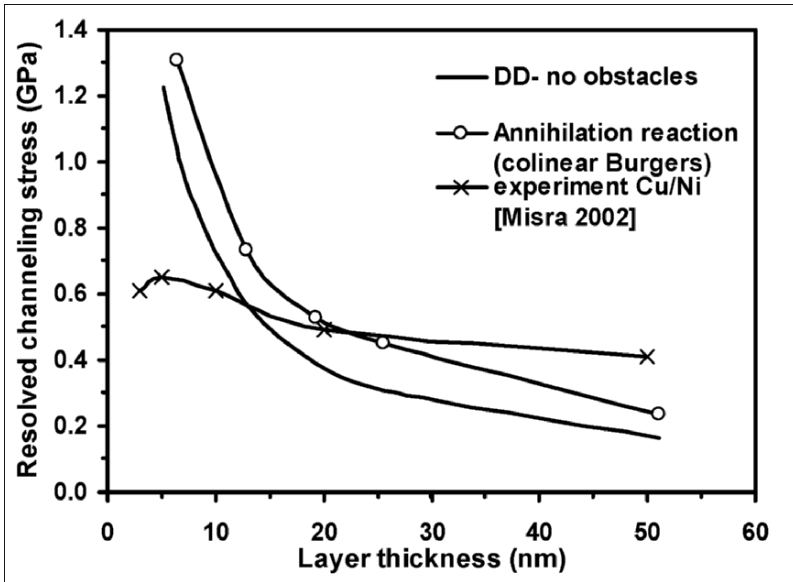


Fig. 6.10. Comparison between DD predictions of the channeling strength due to the basic Orowan bowing and that due to the orthogonal interaction between a threading and an interfacial dislocation of the same Burgers vector (also shown is the experimentally measured strength of Cu/Ni NMM composite)

model are also included. As can be seen from the figure, the strength predictions due to the strongest orthogonal dislocation interactions in NMM composites are significantly higher than those of the reference “plain” Orowan bowing process. Furthermore, they are in better agreement with the measured strength of the Cu/Ni composite system in the range of 22 nm, approximately, and above; while below this range the strength is overestimated.

Together, these observations indicate a model-based collinear orthogonal interaction results in better predictions of strength in NMM composites, although this is still incomplete. In the lower layer thickness structures, the results strongly suggest that softening mechanisms become more significant in governing the response of NMM composites.

### ***Interaction between threading and parallel interfacial dislocations***

Another frequent long-range dislocation interaction in NMM composites is the parallel threading of a dislocation in the vicinity of a predeposited interfacial dislocation and parallel to it. The closer the threading dislocation is to the interfacial dislocation, the stronger will be the effect of the later dislocation on the driving force for threading. Depending on the direction of the Burgers vectors of the two dislocations, the presence of the interfacial dislocation can impede or augment the threading process. Figure 6.11 shows DD results for the thickness dependence of the channeling stress as a function of the spacing (normalized with respect to layer thickness) between the threading and the parallel interfacial dislocation.

As the spacing between the threading dislocation and the predeposited dislocation dipole becomes smaller, the interaction gets stronger. The figure also demonstrates the effect of the relative sense of the Burgers vector of the two dislocations on the channeling strength. The cases identified by “parallel” in Fig. 6.11 refer to the case where the two dislocations have collinear Burgers vectors, while “antiparallel” refers to the case where the two dislocations have opposite Burgers vectors. In the former case, the interaction energy between the threader and the interfacial dislocation is positive, meaning that additional work has to be supplied to overcome the interaction. In the latter case, the interaction energy is negative implying that less work, relative to the “plain” Orowan bowing, needs to be spent. Finally, Fig. 6.11 overlays the measured strength of the Cu/Ni nanocomposite systems for comparison. Besides the significance of their effect on the channeling stress, parallel interactions have important implications on the minimum spacing between parallel interfacial dislocations. A new threader will need to be sufficiently far from a neighboring threader already threaded at an earlier stage in the relaxation process.

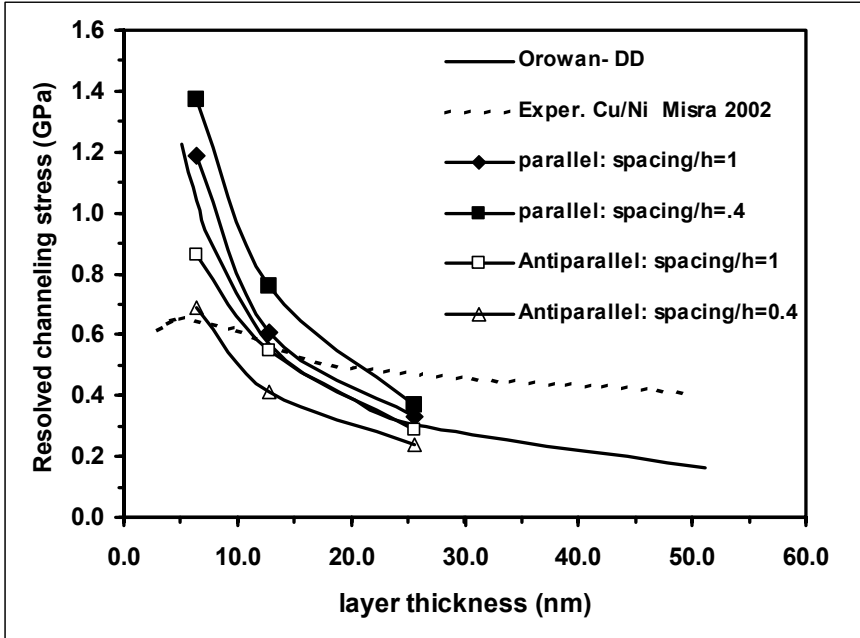


**Fig. 6.11.** Comparison between DD predictions of the channeling strength due to the basic Orowan bowing and that due to the parallel interaction between a threading and an interfacial dislocation of the same Burgers vector (also shown is the experimentally measured strength of Cu/Ni NMM composite)

### ***Threading in surface layer: effect of free surface on threading strength***

In the previous three examples, unit dislocation mechanisms were studied as they occur in a layer embedded in an infinite medium with homogenous elastic properties similar to that of the layer. In this example, the threading process in a surface layer of a large stack is considered. The fundamental difference is that the presence of a free surface will impose an additional stress (image stress) on the threading dislocation.

Image stresses induce an attractive force on dislocations close to the boundary pulling them toward the free surface and out of the medium. As pointed out in Sect. 6.2.3, the multiscale DD model, coupled with FE analysis, rigorously accounts for this effect through the superposition principle and the solution of the complementary elasticity problem, as explained there.

To assess the surface effect, the stress needed to propagate a threading dislocation in a surface layer was estimated with/without the multiscale

coupling with FE analysis enabled. A layer thickness of 25 nm was considered, and the threading dislocation considered had the slip system  $a/2[01-1]$  (111), with the same crystallographic setup as that indicated in Fig. 6.5a. The surface layer and the rest of the domain were subjected to equal but opposite sign stresses as is the case in threading induced by coherency stress during the relaxation process.

It was found that a biaxial stress of 0.4 GPa was necessary to propagate the threader when surface treatment through the multiscale analysis was disabled, while in the case it was enabled, the corresponding stress was 0.2 GPa. This difference is significant and indicates that a free surface enhances the threading process in a surface layer. Further investigation of this effect for a different layer thickness is in progress and will be the subject of a future publication.

#### 6.4.2 Modeling of Dislocation Systems in NMM Composites

Although the understanding of unit dislocation mechanisms is a crucial first step toward predicting the overall response of NMM composites, the complexity of dislocation interactions in real systems makes the task of extending an understanding of isolated units to overall behavior nontrivial, if not impossible. As can be concluded from comparing the measured strength of NMM composites and predicted strength based on parallel and orthogonal interactions between threading and interfacial dislocations (Figs. 6.10 and 6.11), no single mechanism can be claimed to be dominant over the whole range of layer thicknesses. Furthermore, the evolution of the dislocation structure under an extremely complex and continuously evolving stress field can significantly change the dynamics of unit process. For example, DD simulations performed by Pant et al. [32] showed that, while in isolation from other dislocations, two threading dislocations gliding in opposite directions on parallel planes can form a dipole and get stuck. However, a third threading dislocation approaching this dipole on a close parallel plane can “free” one of the dislocations in the existing dipole and form a new dipole. The high density of dislocations in a real system makes it impossible to track the effect on the overall response of the possibly large number of similar interactions between the background dislocations and the unit mechanisms.

The above complexity of the dislocation behavior in NMM composites can be handled using DD analysis because dislocation motion and interactions are treated explicitly. Their motion is directly calculated from the net stress field due to all other dislocations and to any applied loads, while boundary conditions can be rigorously treated through the coupling

to FE. Short-range interactions are also accounted for through physical constitutive rules. Thus, capturing the natural evolution of a real system is possible and feasible in spite of the heavy computational expense. Nevertheless, the question of the validity of such massive simulations hinges on the validity of the initial dislocation structure from which loading starts.

Arriving at a valid initial structure should also be the natural outcome of the process leading to it, i.e., the relaxation process of the as-deposited composite. DD simulations for the relaxation process of an as-deposited NMM structure and its consequent loading are presented in the following sections. The relaxation simulation starts from an initial random distribution of threading dislocations driven by an alternating system of coherency stresses, as suggested by the physics of the deposition and relaxation process in real systems, and ends at the point when the dynamics evolution of the systems ceases, marking the arrival at a relaxed equilibrium structure. The loading simulation starts from this relaxed structure by applying strain rate-controlled uniform biaxial loading. From this simulation, stress–strain curves can be collected from which the strength of the composite is captured.

### ***Modeling of the relaxation process and as-deposited structure***

The goal of these simulations is to arrive at a representative relaxed structure for NMM composites with physical initial dislocation content and residual coherency stresses. The simulation box is made of four layers, and represents an infinite domain made of alternating layers of the bimetal system. To ensure this, periodic boundary conditions are applied to the simulation box in all three directions. Each layer is 12.7 nm thick, and its elastic properties are those of Cu (Table 6.1). All the layers have the same elastic properties; however, they are under a stress field of equal magnitude but alternating sign in alternating layers. The stress field is due to coherency stress resulting from lattice parameters mismatch between the two materials making the alternating layers. Strictly speaking, this setup represents a bimetal system with matching elastic properties but different lattice parameters. However, as was explained earlier, this idealization is still reasonable for the Cu/Ni system.

The coherency stress used in the simulation is 2.6 GPa [16] and is biaxial. The simulation begins with a random distribution of dislocation loops spanning the four layers. If the layer thickness is larger than the critical thickness  $h_c$ , dislocations glide in opposite directions in the alternating layers due to the alternating stress state. In the process, dislocations

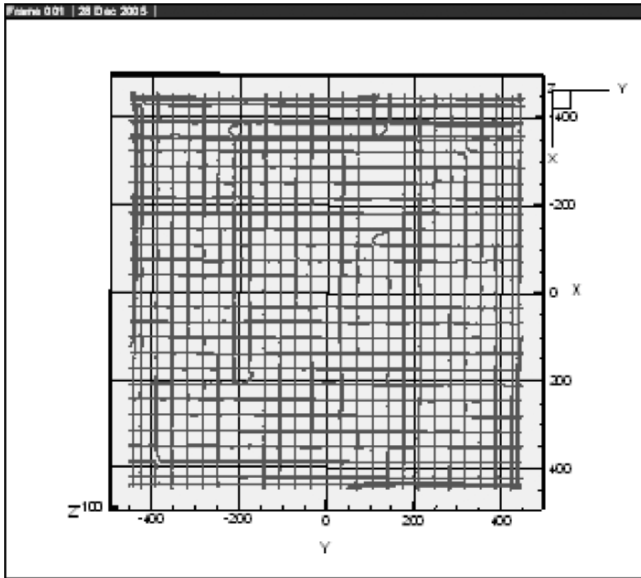
naturally interact with the stress field and among themselves result in the relaxation of the coherency stress and at the expense of generating a new dislocation structure.

The process continues until dislocation motion ceases indicating the attainment of an equilibrium state between the dislocations and the final distribution of internal stress. Figure 6.12 shows DD simulation of the final structure after the relaxation process has ended. As can be seen, the structure consists dominantly of a network of orthogonal interfacial dislocations, dislocation bends resulting from cross-slip, and blocked threading dislocations. Another dislocation mechanism that was observed during the relaxation process but leaves no traces of its occurrence in the final structure is annihilation of threaders of opposite signs. As they do so, the threading segments get eliminated leaving only the trailing hairpin arm at the interfaces.

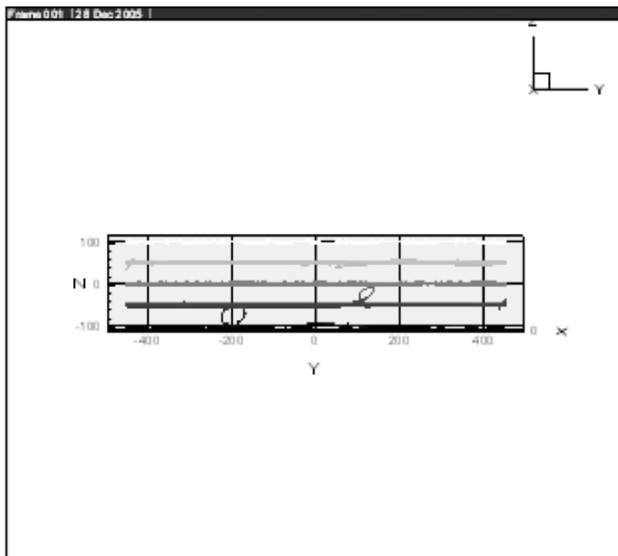
### ***Modeling of the biaxial loading process***

As mentioned previously, the resulting structure at the end of the relaxation process is considered to be representative of that of an as-deposited structure that has relaxed, although incompletely as discussed previously, its coherency stresses through the threading process. To study the strength of NMM composites, this structure serves as the starting point for loading. The same periodic four-layer system used in the relaxation simulation is used here. Tensile biaxial loading at a controlled strain rate is applied.

Figure 6.13a is a side snapshot showing dislocation activity under loading just after the yield point has been reached. It shows that the top and the third-from-top layers, which had compressive coherency stresses in the relaxation phase, are now showing reversal of dislocation activity due to the opposite sign loading. This recovery process is limited to those dislocations which have not undergone irreversible short-range interactions and those which threaded to some length that is short of their threading stability point. The other two layers, which were under tensile coherency stresses in the relaxation process, are showing a resumption of dislocation activity. Figure 6.13b shows the stress evolution curve captured by the simulation. As can be seen, the yield point occurs at about 2.2 GPa. The difference between this value and the 2.6 GPa coherency stress experienced in the relaxation phase reflects the fact that relaxation is not complete due to the impediments to relaxation expected to exist in real systems, as discussed earlier.

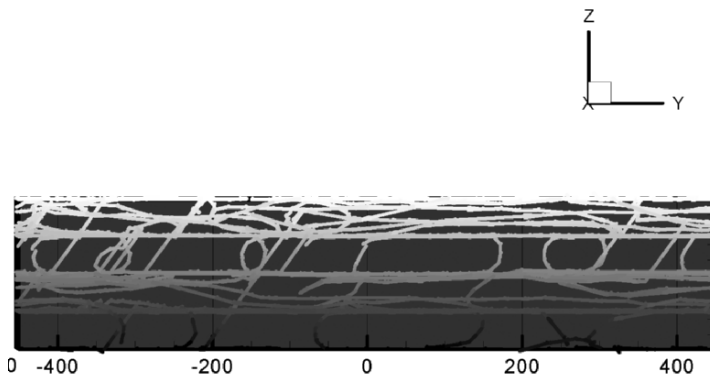


(a)

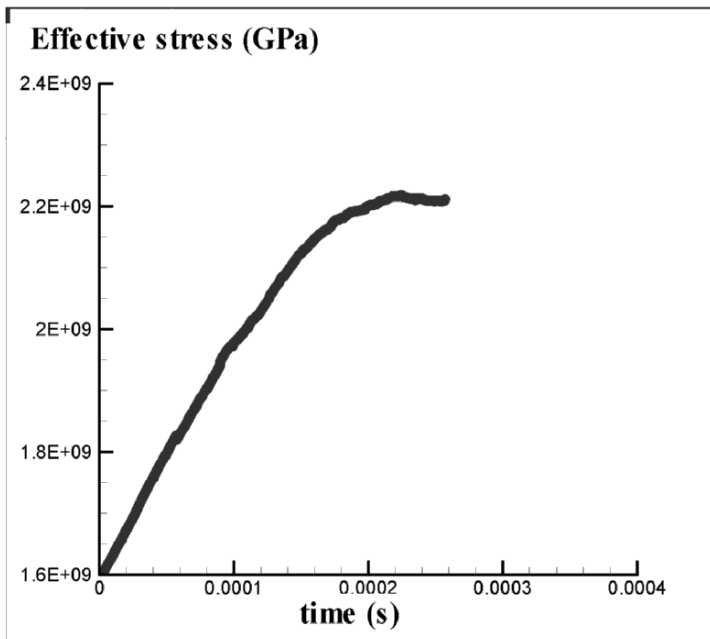


(b)

**Fig. 6.12.** Relaxed dislocation configuration due to coherency stress in a four-layered structure representative of a bimetal multilayered structure



(a)



(b)

**Fig. 6.13.** Biaxial loading of the relaxed multilayer structure shown in Fig. 6.12: (a) side view of the dislocation activity after yielding and (b) stress evolution as captured by the simulation

## References

1. Akasheh F, Zbib HM, Hirth JP, Hoagland RG, Misra A. 2007. Dislocation dynamics analysis of dislocation intersections in nanoscale metallic multilayered composites. *Journal of Applied Physics* 101:084314
2. Bulatov VV, Rhee M, Cai W. 2000. Periodic Boundary Conditions for Dislocation Dynamics Simulations in Three Dimensions. Proceedings of the MRS meeting
3. DeWit R. 1960. The continuum theory of stationary dislocations. *Solid State Physics* 10:249–292
4. Feng X, Hirth JP. 1992. Critical layer thickness for inclined dislocation stability in multilayer structures. *Journal of Applied Physics* 72:1386–1393
5. Fivel MC, Roberston CF, Canova G, Bonlanger L. 1998. Three-dimensional modeling of indent-induced plastic zone at a mesoscale. *Acta Materialia* 46:6183–6194
6. Frank FC, van der Merwe JH. 1949. One-dimensional dislocations. I. Static theory. *Proceedings of the Royal Society of London A* 198:205
7. Freund LB. 1990. A criterion for arrest of a threading dislocation in a strained epitaxial layer due to an interface misfit dislocation in its path. *Journal of Applied Physics* 68:2073–2080
8. Ghoniem NM, Amodeo RJ. 1990. Numerical simulation of dislocation patterns during plastic deformation. In: Walgraef D, Ghoniem NM, editors. *Patterns, Defects and Material Instabilities*. Kluwer, Dordrecht, pp 303–329
9. Gosling TJ, Bullough R, Jain SC, Willis JR. 1993. Misfit dislocation distributions in capped (buried) strained semiconductor layers. *Journal of Applied Physics* 73:8267–8278
10. Gosling TJ, Willis JR, Bullough R, Jain SC. 1993. The energetics of dislocation array stability in strained epitaxial layers. *Journal of Applied Physics* 73:8297–8303
11. Hirth JP. 1992. Injection of dislocations into strained multilayer structures. In: *Semiconductors and Semimetals*. Academic, London, pp 267–292
12. Hirth JP, Feng X. 1990. Critical layer thickness for misfit dislocation stability in multilayer structures. *Journal of Applied Physics* 67:3343–3349
13. Hirth JP, Lothe J. 1982. *Theory of Dislocations*. Wiley, New York, p 857
14. Hirth JP, Zbib HM, Lothe J. 1998. Forces on high velocity dislocations. *Modelling and Simulation in Materials Science and Engineering* 6:165–169
15. Hoagland RG, Hirth JP, Misra A. 2006. On the role of weak interfaces in blocking slip in nanoscale layered composites. *Philosophical Magazine* 86:3537–3558
16. Hoagland RG, Mitchell TE, Hirth JP, Kung H. 2002. On the strengthening effects of interfaces in multilayer fcc metallic composites. *Philosophical Magazine A* 82:643–664
17. Hochbauer T, Misra A, Hattar K, Hoagland RG. 2005. Influence of interfaces on the storage of ion-implanted He in multilayered metallic composites. *Journal of Applied Physics* 98:123516

18. Huang H, Ghoniem N, Diaz de la Rubia T, Rhee M, Zbib HM, Hirth JP. 1999. Development of physical rules for short range interactions in BCC crystals. *ASME-JEMT* 121:143–150
19. Kamat SV, Hirth JP. 1990. Dislocation injection in strained multilayer structures. *Journal of Applied Physics* 67:6844–6850
20. Koehler JS. 1970. Attempt to design a strong solid. *Physical Review B* 2:547–551
21. Kubin LP, Canova G. 1992. The modelling of dislocation patterns. *Scripta Metallurgica* 27:957–962
22. Mara N, Sergueeva A, Misra A, Mukherjee AK. 2004. Structure and high-temperature mechanical behavior relationship in nano-scaled multilayered materials. *Scripta Materialia* 50:803–806
23. Matthews JW, Blakeslee AE. 1974. Defects in epitaxial multilayers. I. Misfit dislocations. *Journal of Crystal Growth* 27:118–125
24. Matthews JW, Mader S, Light TB. 1970. Accommodation of misfit across the interface between crystals of semiconducting elements or compounds. *Journal of Applied Physics* 41:3800–3804
25. Misra A, Hirth JP, Hoagland RG, Embury DJ, Kung H. 2004. Dislocation mechanisms and symmetric slip in rolled nano-scaled metallic multilayers. *Acta Materialia* 52:2387–2394
26. Misra A, Hirth JP, Kung H. 2002. Single-dislocation-based strengthening mechanisms in nanoscale metallic multilayers. *Philosophical Magazine A* 82:2935–2951
27. Misra A, Hoagland RG. 2005. Effects of elevated temperature annealing on the structure and hardness of copper/niobium nanolayered films. *Journal of Materials Research* 20:2046–2054
28. Misra A, Kung H. 2001. Deformation behavior of nanostructured metallic multilayers. *Advanced Engineering Materials* 3:217–222
29. Mitlin D, Misra A, Mitchell TE, Hoagland RG, Hirth JP. 2004. Influence of overlayer thickness on the density of Lomer dislocations in nanoscale Ni–Cu bilayer thin films. *Applied Physics Letters* 85:1686–1688
30. Mitlin D, Misra A, Radmilovic V, Nastasi M, Hoagland RG, Embury D, Hirth JP, Mitchell T. 2004. Formation of misfit dislocations in nanoscale Ni–Cu bilayer films. *Philosophical Magazine* 84:719–736
31. Nix WD. 1998. Yielding and strain hardening of thin metal films on substrates. *Scripta Materialia* 39:545–554
32. Pant P, Schwarz KW, Baker SP. 2003. Dislocation interactions in thin FCC metal films. *Acta Materialia* 51:3243–3258
33. Schwarz KW, Tersoff J. 1996. Interaction of threading and misfit dislocations in a strained epitaxial layer. *Applied Physics Letters* 69:1220–1222
34. Van der Giessen E, Needleman A. 1995. Discrete dislocation plasticity: a simple planar model. *Materials Science and Engineering* 3:689–735
35. Wang YC, Misra A, Hoagland RG. 2006. Fatigue properties of nanoscale Cu/Nb multilayers. *Scripta Materialia* 54:1593–1598

36. Willis JR, Jain SC, Bullough R. 1990. The energy of an array of dislocations: implications for strain relaxation in semiconductor heterostructures. *Philosophical Magazine A* 62:115–129
37. Yasin H, Zbib HM, Khaleel MA. 2001. Size and boundary effects in discrete dislocation dynamics: coupling with continuum finite element. *Materials Science and Engineering A* 309–310:294–299
38. Zbib HM, Diaz de la Rubia TA. 2001. Multiscale Model of Plasticity: Patterning and Localization. *Material Science for the 21st Century*, The Society of Materials Science, Japan, Vol. A, pp 341–347
39. Zbib HM, Diaz de la Rubia T. 2002. A multiscale model of plasticity. *International Journal of Plasticity* 18:1133–1163
40. Zbib HM, Rhee M, Hirth JP. 1996. 3D simulation of curved dislocations: discretization and long range interactions. In: Abe T, Tsuta T, editors. *Advances in Engineering Plasticity and Its Applications*. Pergamon, Amsterdam, pp 15–20
41. Zbib HM, Rhee M, Hirth JP. 1998. On plastic deformation and the dynamics of 3D dislocations. *International Journal of Mechanical Science* 40:113–127